
Article:
Lazarov, Vlado orcid.org/0000-0002-4314-6865, Kuerbanjiang, Balati orcid.org/0000-0001-6446-8209, Ghasemi, Arsham et al. (8 more authors) (2018) Correlation between spin transport signal and Heusler/semiconductor interface quality in lateral spin-valve devices. Physical Review B. 115304. ISSN 2469-9969

https://doi.org/10.1103/PhysRevB.98.115304

Supplementary Materials: Correlation between spin transport signal and Heusler/semiconductor interface quality in lateral spin-valve devices

B. Kuerbanjiang,[1] Y. Fujita,[2] M. Yamada,[2] S. Yamada,[2,3] A. Ghasemi,[1] P. J. Hasnip,[1] A. M. Sanchez,[4] D. Kepaptsoglou,[5] G. Bell,[4] K. Sawano,[6] K. Hamaya[2,3] and V. K. Lazarov[1]

[1] *Department of Physics, University of York, York YO10 5DD, United Kingdom.*
[2] *Graduate School of Engineering Science, Osaka University, 1-3 Machikaneyama, Toyonaka 560-8531, Japan.*
[3] *Center for Spintronics Research Network, Osaka University, 1-3 Machikaneyama, Toyonaka 560-8531, Japan.*
[4] *Department of Physics, University of Warwick, Coventry CV4 7AL, United Kingdom.*
[5] *SuperSTEM laboratory, SciTeck Daresbury Campus, Daresbury WA4 4AD, United Kingdom.*
[6] *Advanced Research Laboratories, Tokyo City University, 8-15-1 Todoroki, Tokyo 158-0082, Japan.*

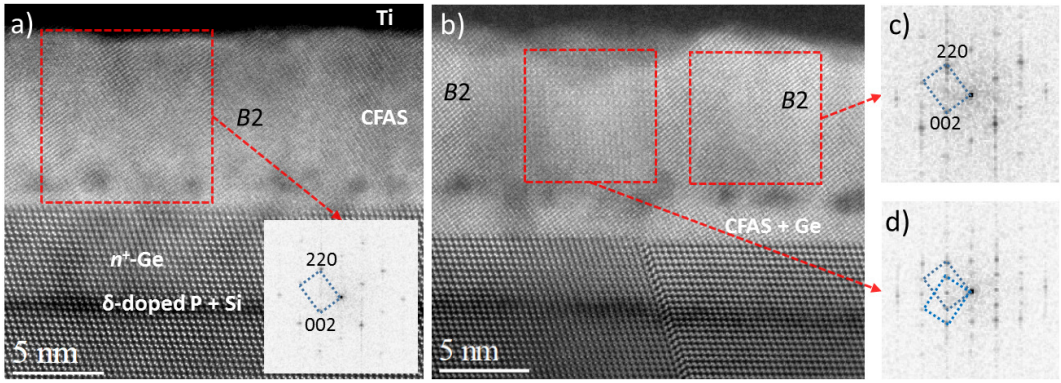

FIG. S1. (Colour online) HAADF-STEM images of the as-prepared (a) and the annealed specimen (b) viewed along $(1\bar{1}0)$ zone axis, respectively. The inset in (a) is a diffractogram of the CFAS film in the outlined area (red dashed square) shows a distinct $B2$ phase. Diffractograms of two crystalline domains in (b) are shown in (c) and (d).

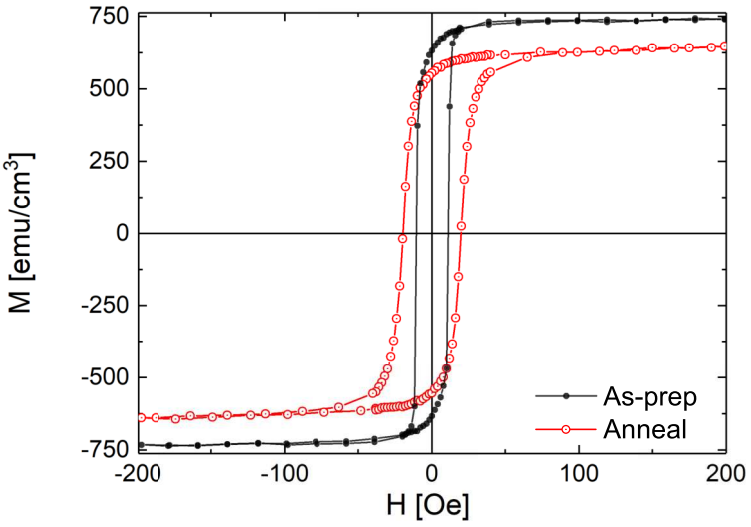

FIG. S2. (Colour online) (a) Hysteresis loops of LSVs in as-prepared state (dotted lines) and after annealing at 300 °C (hollow circles).

FIG. S3 shows the band gap of 0.6 eV for minority (spin down states, FIG. S3 (a)). Note that the increase of disorder (incorporation of Ge in CFAS by substitution of Co) mainly affects the spin down states, which provide the band gap for one of the spin channel. This is due to decreased in electron correlation between Co atoms on the same

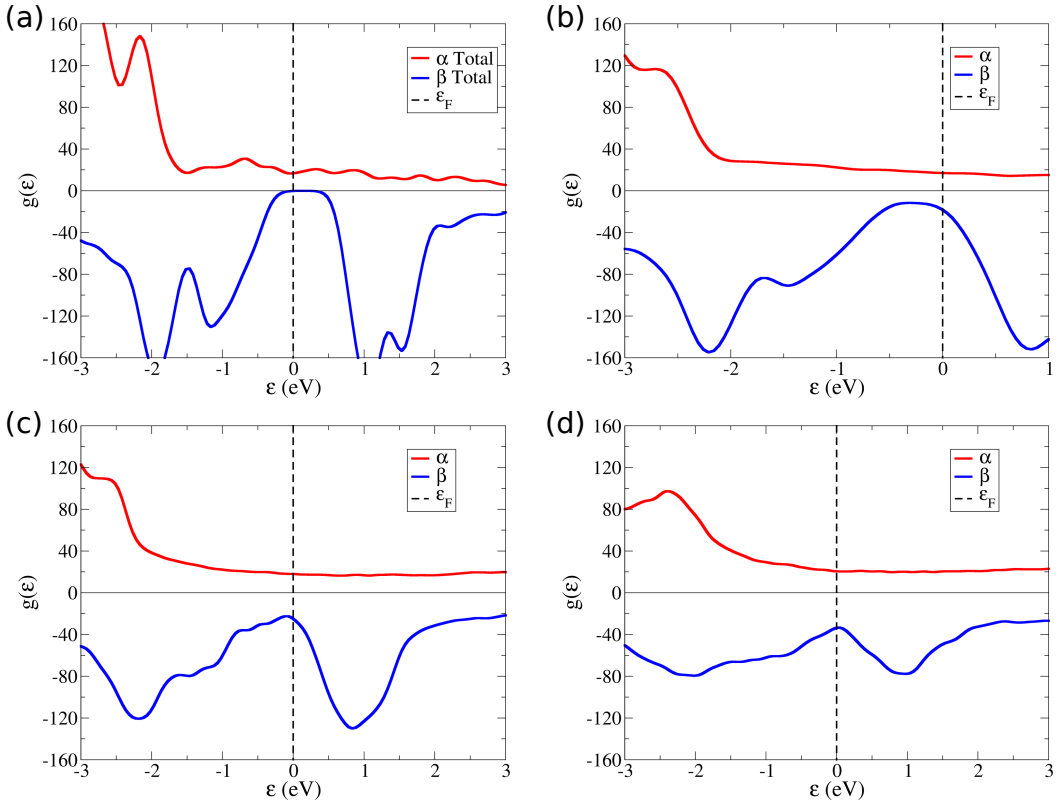

FIG. S3. (Colour online) a) Spin density of states of bulk CFAS. Spin density of states for disordered CFAS, where Ge substitutes Co for the concentrations of 12.5% (b), 25% (c), and 50% (d). α and β represent spin up and spin down states, respectively.

sublattice (8c sites), and Co-Fe sublattices, which results in decrease of hybridisation/localisation of the d orbitals around the Fermi level. The increased number of states in spin down channel eventually kills the spin polarisation at the Fermi level, $\sim$ 15% of Ge substitution of Co. Examples of spin-DOS for 12.5%, 25%, and 50% substitu-tion of Co by Ge are presented in FIG. S3 (b), (c), and (d), respectively.

Ge substitution of Co atoms changes drastically the spin density of states of the spin down channel (β) at the Fermi level. FIG. S4 shows a presence of the negative spin polarisation at the Fermi level. Note that disorder mainly affects the spin down channel, and that the states are dominantly due to Co.

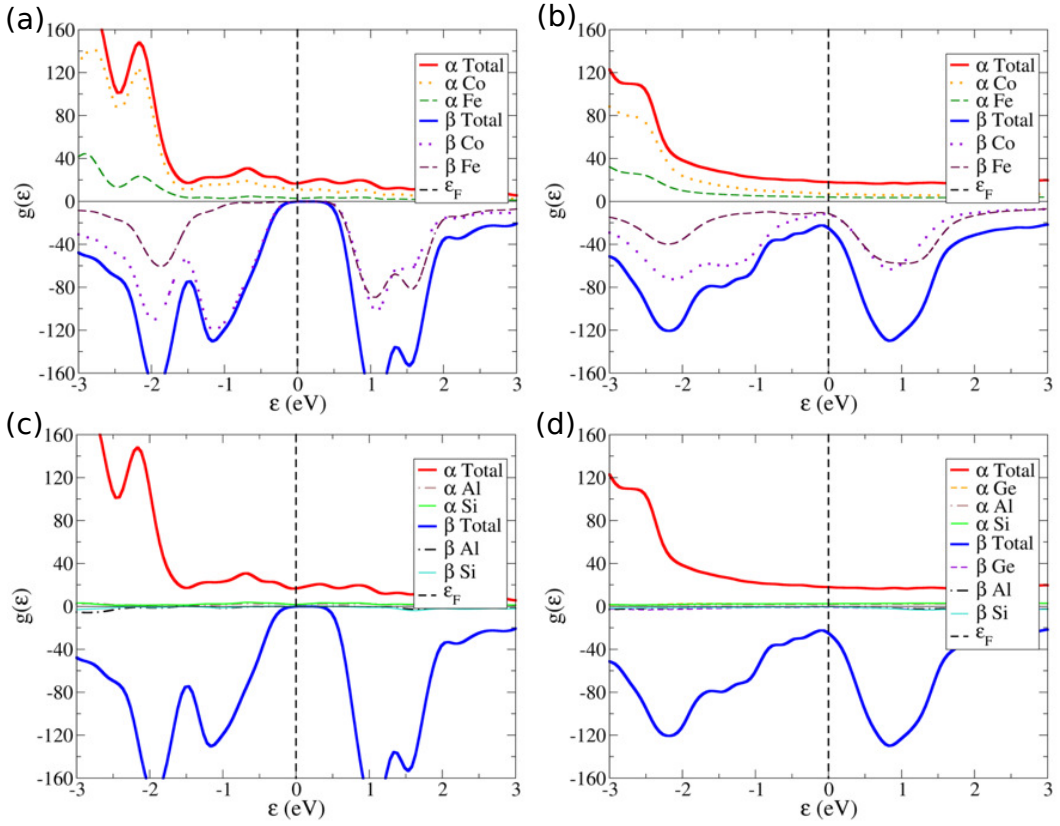

FIG. S4. (Colour online) Partial spin density of states for pure CFAS (a, c) and CFAS where Ge substitutes 25% of Co (b, d). In both cases almost all the states near the Fermi level come from Co and Fe (a, b), with Al, Si and Ge hardly contributing (c, d).

TABLE S1: Extended results of first-principles calculations showing the dependence of the magnetic moment M and spin polarisation P as a function of the concentration of Ge substituting atoms in CFAS. n(Si), n(Al), n(Fe), n(Co) and n(Ge) stand for the number of Si, Al, Fe, Co and Ge, respectively, in a considered configuration. The first row represents bulk CFAS where the unit cell has 16 atoms. Note that using a general X_2YZ formula for full Heusler alloys, X represents the sublattice of Co, Y sublattice of Fe, and Z the sublattice of Al/Si.

Label	n(Si)	n(Al)	n(Fe)	n(Co)	n(Ge)	M [μ_B/u.c.]	P[%]
Bulk	16	16	32	64	0	176.0	100
Z1	15	16	32	64	1	176.0	100
Z2	14	16	32	64	2	176.0	100
Z3	13	16	32	64	3	176.0	100
Z4	12	16	32	64	4	176.1	100
Z5	11	16	32	64	5	176.1	100
Z6	10	16	32	64	6	176.1	100
Z7	9	16	32	64	7	176.1	100
Z8	8	16	32	64	8	176.1	100
Z9	7	16	32	64	9	176.1	100
Z10	6	16	32	64	10	176.2	100
Z11	5	16	32	64	11	176.2	100
Z12	4	16	32	64	12	176.2	100
Z13	3	16	32	64	13	176.3	100
Z14	2	16	32	64	14	176.3	100
Z15	1	16	32	64	15	176.3	100
Z16	0	16	32	64	16	176.4	100
Z17	16	15	32	64	17	177.0	100
Z18	16	14	32	64	18	178.0	100
Z19	16	13	32	64	19	179.0	100
Z20	16	12	32	64	20	180.0	100
Z21	16	11	32	64	21	181.0	100
Z22	16	10	32	64	22	182.0	100
Z23	16	9	32	64	23	183.0	100
Z24	16	8	32	64	24	184.0	100
Z25	16	7	32	64	25	185.0	100
Z26	16	6	32	64	26	186.0	100
Z27	16	5	32	64	27	187.0	100
Z28	16	4	32	64	28	188.0	100
Z29	16	3	32	64	29	189.0	100
Z30	16	2	32	64	30	190.0	100
Z31	16	1	32	64	31	191.0	100
Z32	16	0	32	64	32	192.0	100
Y1	16	16	31	64	1	172.0	100
Y2	16	16	30	64	2	168.0	100
Y3	16	16	29	64	3	164.1	100
Y4	16	16	28	64	4	160.1	100
Y5	16	16	27	64	5	156.1	100
Y6	16	16	26	64	6	152.1	100
Y7	16	16	25	64	7	148.2	100
Y8	16	16	24	64	8	144.4	99
Y9	16	16	23	64	9	140.5	94
Y10	16	16	22	64	10	136.7	86
Y11	16	16	21	64	11	132.7	87
Y12	16	16	20	64	12	129.1	67
Y13	16	16	19	64	13	125.3	63
Y14	16	16	18	64	14	121.5	62
Y15	16	16	17	64	15	117.7	60
Y16	16	16	16	64	16	114.0	56
Y17	16	16	15	64	17	110.4	59
Y18	16	16	14	64	18	106.6	65
Y19	16	16	13	64	19	103.0	76

Continued

TABLE S1 – continued

Y20	16	16	12	64	20	99.2	66
Y21	16	16	11	64	21	95.3	70
Y22	16	16	10	64	22	91.4	63
Y23	16	16	9	64	23	87.5	64
Y24	16	16	8	64	24	83.7	39
Y25	16	16	7	64	25	79.8	22
Y26	16	16	6	64	26	75.8	17
Y27	16	16	5	64	27	71.9	12
Y28	16	16	4	64	28	68.0	9
Y29	16	16	3	64	29	64.1	6
Y30	16	16	2	64	30	60.3	8
Y31	16	16	1	64	31	56.3	9
Y32	16	16	0	64	32	52.3	45
X1	16	16	32	63	1	177.0	100
X2	16	16	32	62	2	178.0	100
X3	16	16	32	61	3	178.6	97
X4	16	16	32	60	4	177.8	100
X5	16	16	32	59	5	177.5	49
X6	16	16	32	58	6	175.3	51
X7	16	16	32	57	7	175.1	14
X8	16	16	32	56	8	173.6	20
X9	16	16	32	55	9	172.2	17
X10	16	16	32	54	10	169.9	-4
X11	16	16	32	53	11	166.5	33
X12	16	16	32	52	12	164.4	-6
X13	16	16	32	51	13	161.3	-16
X14	16	16	32	50	14	156.9	-14
X15	16	16	32	49	15	154.1	-19
X16	16	16	32	48	16	150.1	-16
X17	16	16	32	47	17	145.3	-9
X18	16	16	32	46	18	141.5	-7
X19	16	16	32	45	19	140.6	-16
X20	16	16	32	44	20	133.6	4
X21	16	16	32	43	21	132.5	-12
X22	16	16	32	42	22	127.7	-3
X23	16	16	32	41	23	123.1	-23
X24	16	16	32	40	24	122.0	-15
X25	16	16	32	39	25	115.3	-13
X26	16	16	32	38	26	112.4	-9
X27	16	16	32	37	27	1 07.4	-15
X28	16	16	32	36	28	101.0	-17
X29	16	16	32	35	29	98.1	-22
X30	16	16	32	34	30	95.4	-26
X31	16	16	32	33	31	87. 1	-25
X32	16	16	32	32	32	94.6	-21.5